Analysis of CLL Voltage-Output Resonant Converters Using Describing Functions

Martin P. Foster, Christopher R. Gould, Adam J. Gilbert, David A. Stone, and Christopher M. Bingham

***Abstract*—A new ac equivalent circuit for the CLL voltage-output resonant converter is presented, that offers improved accuracy compared with traditional FMA-based techniques. By employing describing function techniques, the nonlinear interaction of the parallel inductor, rectifier and load is replaced by a complex impedance, thereby facilitating the use of ac equivalent circuit analysis methodologies. Moreover, both continuous and discontinuous rectifier-current operating conditions are addressed. A generic normalized analysis of the converter is also presented. To further aid the designer, error maps are used to demonstrate the boundaries for providing accurate behavioral predictions. A comparison of theoretical results with those from simulation studies and experimental measurements from a prototype converter, are also included as a means of clarifying the benefits of the proposed techniques.**

***Index Terms*—DC–DC power conversion, modeling, resonant power conversion.**

I. Introduction

With the recent changes in the world climate being attributed to global warming and the depletion of fossil fuels, energy conservation is becoming of paramount concern. In response to this need, the designers of power supplies for industrial, commercial and domestic market sectors are continually searching for technologies which meet their systems' requirements while simultaneously achieving higher operating efficiencies. Resonant power converters have been recognized as a viable technology in this pursuit by virtue of providing: 1) zero-voltage switching (ZVS) and/or zero current switching (ZCS) of the power devices; 2) a reduction in component sizes; and 3) the incorporation of the normally detrimental effects of parasitic elements, as design components (transformer leakage and magnetising inductances, and inter-winding capacitances being primary candidates), thereby further improving power density. Owing to these properties, resonant converter technologies are finding their way into all manner of applications including consumer electronic devices and high-power factor telecommunications supplies [1], automotive battery charging [2] and fuel cell backup supplies [3], as well as capacitor charging for pulsed power applications [4]. However, the complex interaction between the resonant circuit, rectifier and load result in a nonlinear output voltage characteristic that is a function of frequency (the control input), thereby making output voltage predictions and converter designs that are robust to component tolerances time-consuming, difficult, and cumbersome. Such factors have therefore impeded the widespread adoption of resonant converter supplies primarily due to the lack of viable mathematical models that can be rapidly employed during the design and evaluation process, except in niche market sectors such as for lamp ballasts.

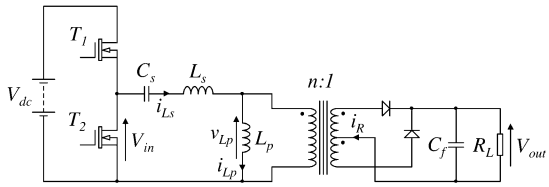

Fig. 1. CLL voltage-output converter.

The paper focuses on enhanced techniques to facilitate the modelling, rapid analysis and design of the CLL resonant converter. This converter type is a member of the more generic LCLC class, and has found particular favour by virtue of the required resonant tank inductors being conveniently formed from the leakage and magnetising inductances of a transformer (see Fig. 1), while providing a ZVS load-independent operating point above resonance [5]—a particularly attractive feature for applications requiring a constant output voltage/constant input voltage/variable load characteristic. Indeed, this topology has recently emerged in some consumer electronics products for the reasons given above.

As discussed, accurately predicting the behavior of CLL converters is complicated by the nonlinear relationship of the output voltage with excitation (input voltage and switching frequency) and load. Consequently, designers often resort to transient-based simulation packages, such as SPICE, to accurately predict the behavior, at the expense of substantial simulation time. In an attempt to expedite the design process, fundamental mode approximation (FMA) has been extensively adopted for the analysis of various resonant converter topologies [5]–[7]. However, while FMA assumes that all circuit voltages and currents take on a sinusoidal waveshape, thereby permitting standard ac circuit analysis techniques to be employed, its accuracy is compromised for nonsinusoidal and nonsquare waveform shapes, as found in the behavior of the CLL converter variant. This disadvantage of FMA has been widely reported, and has resulted in several studies that have developed models based on the steady-state solution of the underlying state-variable equations that accurately describe resonant circuit behavior [8]–[10]. While the results of these models can be very accurate, they are often difficult

Manuscript received June 25, 2007; revised October 18, 2007. Published July 7, 2008 (projected). This work was supported by the Engineering and Physical Sciences Research Council and the Nuffield Foundation. Recommended for publication by Associate Editor R.-L. Lin.

The authors are with the Department of Electronic and Electrical Engineering, The University of Sheffield, Sheffield S1 3JD, U.K. (e-mail: m.p.foster@sheffield.ac.uk).

Color versions of one or more of the figures in this paper are available online at http://ieeexplore.ieee.org.

Digital Object Identifier 10.1109/TPEL.2008.924835

to implement and interpret, and recourse to the use of design charts and/or numerical type solutions to realize a design, is commonplace.

This paper specifically presents a modelling methodology for the CLL voltage-output converter developed using describing function techniques, where the voltage across the parallel inductor, v_{Lp}, and current through the rectifier, i_R, is more accurately described. A similar technique has previously been successfully applied to model the LCC voltage-output converter [11]–[14] and the LCC current-output converter operating under heavy load conditions [15]. The presented analysis is based on an approximate model for the CLL converter previously reported in [16] where the waveform shape of i_R is approximated by a half-wave rectified sinusoid with dead-periods. An improvement on this is now reported by employing a more detailed description for the waveform characteristics. Specifically, it is assumed that i_{Ls} takes on a sinusoidal form and that v_{Lp} and i_R can be decomposed into a set of piecewise equations that more accurately describe their waveshapes. Applying a Fourier transformation to these waveforms and extracting the fundamental permits the development of an equivalent circuit model with demonstrably improved accuracy.

II. Description of Converter Operation

Referring to Fig. 1, the half-bridge MOSFETs T_1 and T_2 are switched in anti-phase at a frequency f_s to produce a squarewave input excitation voltage $V_{\rm in}$. This voltage excites the resonant tank, causing a current i_{Ls} to flow. When the rectifier is conducting, v_{Lp} is clamped by $V_{\rm out}$ and current flows from the resonant circuit into C_f, replenishing the charge and dictating the output voltage. If, immediately after the rectifier turn-off commutation, $|v_{Lp}|$ is greater than $nV_{\rm out}$, then the rectifier turns-on. During these conditions the converter is said to be operating in continuous rectifier current mode, and v_{Lp} can be considered a square waveform—see Fig. 2(a). However, for certain excitation/loading conditions (as discussed in Section III-C) $|v_{Lp}| < nV_{\rm out}$ and the rectifier remains off for a significant portion of the switching half-cycle. During this "nonconduction period" [α in Fig. 2(b)] all of i_{Ls} flows through L_p, and v_{Lp} then takes on a cosine characteristic—the converter is then considered to be operating in a discontinuous rectifier current condition mode. The effect of the nonconduction period is to significantly alter the effective resonant frequency and effective Q-factor of the supply, enabling 'boosting' of the output voltage.

III. Derivation of Equivalent Circuit Models

It is now assumed that the input current is sinusoidal—the justification for this being that the tank circuit is essentially a band-pass filter and significantly attenuates all harmonics other than the resonant frequency. Thus, it is reasonable to assume that

$$i_{Ls} = I_{\rm in}\sin(\omega_s t) = I_{\rm in}\sin(\theta) \tag{1}$$

(Note: to simplify notation $\omega_s t$ is normalized by 2π to an angle θ throughout.)

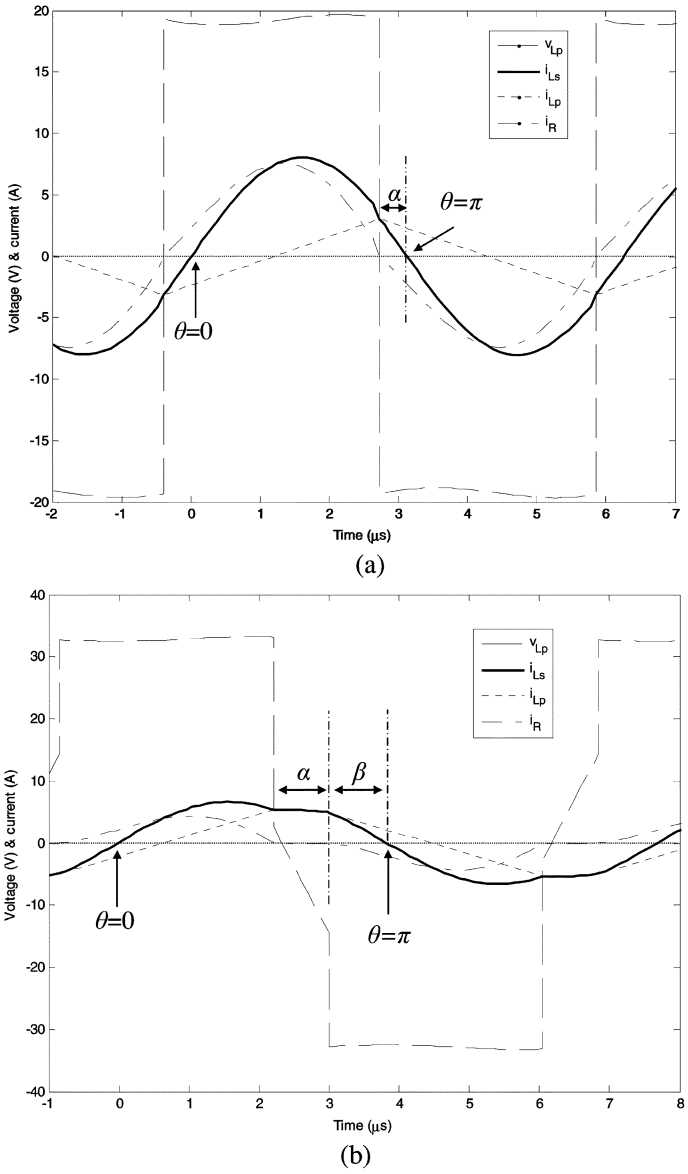

Fig. 2. Resonant circuit voltage and current waveforms: (a) operation with continuous i_R and (b) operation with discontinuous i_R.

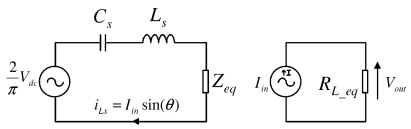

Fig. 3. Equivalent circuit of CLL voltage-output converter.

In the analyses that follow, the parallel inductor, rectifier and output filter are replaced by an equivalent impedance, $Z_{\rm eq}$. An expression for $Z_{\rm eq}$ is derived by describing the parallel inductor voltage v_{Lp} by its fundamental component (v_{Lp_1}) and dividing by the current flowing through the resonant circuit (i_{Ls}). $Z_{\rm eq}$ is subsequently combined with L_s and C_s to form an AC equivalent circuit model of the converter, see Fig. 3. The magnitude of the input current, $I_{\rm in}$, is then determined using Ohm's law, and is employed as an equivalent current source to determine $V_{\rm out}$. Essential to this activity is the determination of switching instants and signal amplitudes to facilitate the description of v_{Lp}

by piecewise equations. Once achieved, v_{Lp} can be expanded using a Fourier series from which the fundamental v_{Lp_1} can be extracted.

A. Operation With Continuous i_R Conduction

When operating in this condition [Fig. 2(a)] v_{Lp} is clamped to $\pm nV_{\rm out}$ for the whole cycle period and v_{Lp} can be seen to lag i_{Ls} by an angle α. Thus, v_{Lp} can be described by a piecewise equation relating the different circuit configurations to the component waveform shapes and phase angles. This expression can be suitably manipulated using a Fourier series to develop the complex, equivalent impedance $Z_{\rm eq}$ that describes the interaction of L_p with R_L via the rectifier. Ultimately, this leads to an expression for the output voltage from knowledge of the average current flow through the rectifier.

Since i_R is continuous, v_{Lp} must be clamped to $V_{\rm out}$ via the rectifier. The parallel inductor voltage is therefore described by

$$v_{Lp}(\theta) = \begin{cases} nV_{\rm out}, & 0 < \theta \le \pi - \alpha \\ -nV_{\rm out}, & \pi - \alpha < \theta \le 2\pi - \alpha \\ nV_{\rm out}, & 2\pi - \alpha < \theta \le 2\pi \end{cases}. \quad (2)$$

The current flowing through the parallel inductor i_{Lp} is determined by integrating v_{Lp} (2) to give (3), as shown at the bottom of the page, where $i_{Lp}(i)$ is the initial condition of the $(i+1)^{th}$ operating mode—$i_{Lp}(0)$ is found from the solution of $i_{Lp}(\pi-\alpha)$ to obtain an expression for the initial condition $i_{Lp}(1)$ in terms of $i_{Lp}(0)$. Substituting for $i_{Lp}(1)$ in $i_{Lp}(0) = -i_{Lp}(\pi)$ the initial condition is found, $i_{Lp}(0) = (nV_{\rm out})/(2\omega_s L_p)(2\alpha - \pi)$.

$V_{\rm out}$ is determined by evaluating the average current flowing through the rectifier during a half-cycle. Thus, evaluating the following integral over a half-cycle, we have

$$\begin{aligned} I_{\rm out} &= \frac{1}{\pi}\int_0^{\pi} |i_R| d\theta = \frac{1}{\pi}\int_0^{\pi} \left(|I_{\rm in}\sin(\theta) - i_{Lp}(\theta)|\right) d\theta \\ &= \frac{1}{\pi}\int_0^{\pi-\alpha} \left(I_{\rm in}\sin(\theta) - i_{Lp1}\sin(\theta)\right) d\theta \\ &\quad - \frac{1}{\pi}\int_{\pi-\alpha}^{\pi} \left(I_{\rm in}\sin(\theta) - i_{Lp2}\sin(\theta)\right) d\theta. \end{aligned} \quad (4)$$

After suitable substitution, this leads to the output current

$$I_{\rm out} = \frac{2nI_{\rm in}\cos(\alpha)}{\pi} \quad (5)$$

and using Ohm's law, the output voltage is given by

$$V_{\rm out} = \frac{2nI_{\rm in}R_L\cos(\alpha)}{\pi} = I_{\rm in}R_{L\_{\rm eq}1} \quad (6)$$

Before $I_{\rm in}$, and hence $V_{\rm out}$, can be determined, the rectifier commutation angle α and the equivalent impedance $Z_{\rm eq}$ (see Fig. 3) must be known. The angle α is found by noting that $i_R(\pi - \alpha) = 0$. Substituting for i_{Ls} and i_{Lp} and after suitable manipulation leads to

$$\alpha = \tan^{-1}\left(\frac{n^2R_L}{\omega_s L_p}\right) = \tan^{-1}\left(\frac{\omega_{0s}}{AQ_s\omega_s}\right) = \tan^{-1}\left(\frac{1}{\lambda}\right) \quad (7)$$

where

$$A = \frac{L_p}{L_s}, \omega_{0s} = \frac{1}{\sqrt{L_sC_s}}, Q_s = \frac{\omega_{0s}L_s}{n^2R_L}, \lambda = \frac{AQ_s\omega_s}{\omega_{0s}}.$$

The equivalent impedance $Z_{\rm eq}$ is obtained by taking the Fourier transform of (2) and extracting the fundamental to provide a describing function approximation for v_{Lp}. Performing a Fourier series expansion on (2), the fundamental component v_{Lp_1} is obtained as

$$v_{Lp\_1} = \frac{4nV_{\rm out}}{\pi}(\sin(\alpha)\cos(\theta) + \cos(\alpha)\sin(\theta)). \quad (8)$$

Substituting for $V_{\rm out}$, dividing by the tank input current (1) and after rearrangement, the equivalent impedance is given by

$$Z_{\rm eq} = \frac{8n^2R_L\cos(\alpha)}{\pi^2}(\cos(\alpha) + j\sin(\alpha)). \quad (9)$$

Finally, the resonant circuit input current $I_{\rm in}$ is found from the total circuit impedance $Z_{\rm tot} = Z_{\rm eq} + j\omega_s L_s + 1/(j\omega_s C_s)$ and using the fundamental component of the tank input voltage as follows:

$$I_{\rm in} = \frac{2V_{\rm dc}}{\pi|Z_{\rm tot}|}. \quad (10)$$

B. Operation With Discontinuous i_R Conduction

This is similar to Section III-A, where a description for v_{Lp} is developed. However, the addition of the nonconduction period significantly complicates the analysis. The waveshape of v_{Lp} is now described by five equations with three representing the rectifier clamping action and a further two describing the rectifier nonconduction periods. A consequence of these extra periods is that expressions for $V_{\rm out}$ and $Z_{\rm eq}$ are now also a function of the two angles α and β [see Fig. 2(b)]. The angles α and β are not determined analytically, but using numerical methods by solving two nonlinear simultaneous equations.

During the rectifier conduction period $|v_{Lp}| = nV_{\rm out}$. During periods of nonconduction, all of the series current i_{Ls} flows through L_p, and $v_{Lp} = \omega_s L_p I_{\rm in}\cos(\theta)$. Combining these leads

$$i_{Lp}(\theta) = \begin{cases} i_{Lp1}(\theta) = \frac{nV_{\rm out}}{\omega_s L_p}\theta + i_{\rm Lp}(0) & 0 < \theta \le \pi - \alpha \\ i_{Lp2}(\theta) = -\frac{nV_{\rm out}}{\omega_s L_p}(\theta - \pi + \alpha) + i_{\rm Lp}(1) & \pi - \alpha < \theta \le 2\pi - \alpha \\ i_{Lp3}(\theta) = \frac{nV_{\rm out}}{\omega_s L_p}(\theta - 2\pi + \alpha) + i_{\rm Lp}(2) & 2\pi - \alpha < \theta \le 2\pi \end{cases} \quad (3)$$

to the description of the whole cycle, as shown in (11), at the bottom of the page.

The parallel inductor current is found by integrating v_{Lp}, as shown in (12), also found at the bottom of the page, where $i_{Lp}(i)$ is the initial condition for the $(i+1)^{th}$ subcircuit.

The initial condition $i_{Lp}(0)$ is found from symmetry by evaluating i_{Lp} at $\theta = \pi$. In practice, this is accomplished by describing i_{Lp} as a straight-line which is fitted to the following values $i_{Lp}(\pi-\beta) = I_{\text{in}}\sin(\beta)$ and $i_{Lp}(2\pi-\alpha-\beta) = I_{\text{in}}\sin(\alpha+\beta)$. The conditions $i_{Lp}(1)$ and $i_{Lp}(3)$ are conveniently accommodated by the sinusoidal term and thus can be set to zero. From Fig. 2(b), it can be seen that $i_{Lp}(2)$ is the final condition of the second operating mode. $i_{Lp}(4)$ is realized using the converter's half-cycle anti-symmetry

$$\begin{aligned} i_{Lp}(0) &= I_{\text{in}}[\beta\sin(\alpha+\beta) + (\alpha+\beta-\pi)\sin(\beta)] \\ i_{Lp}(2) &= I_{\text{in}}\sin(\beta) = -i_{Lp}(4). \end{aligned} \tag{13}$$

As shown previously in (4), an expression for I_{out} can be developed by evaluating the average current flowing through the rectifier. Over one half-cycle

$$\begin{aligned} I_{\text{out}} &= \frac{1}{\pi}\int_0^{\pi-\alpha-\beta}(I_{\text{in}}\sin(\theta) - i_{Lp1}\sin(\theta))d\theta \\ &\quad - \frac{1}{\pi}\int_{\pi-\beta}^{\pi}(I_{\text{in}}\sin(\theta) - i_{Lp3}\sin(\theta))d\theta \\ &= \frac{nI_{\text{in}}}{\pi}[\cos(\alpha+\beta) + (\pi-\alpha)\sin(\beta) + \cos(\beta)] \\ &\quad - \frac{n^2V_{\text{out}}}{2\pi\omega_s L_p}(\pi-\alpha)^2. \end{aligned} \tag{14}$$

Substituting for V_{out} and rearranging provides

$$\begin{aligned} I_{\text{out}} = \frac{2\lambda n}{2\pi\lambda + (\alpha-\pi)^2}I_{\text{in}} \\ \cdot[(\pi-\beta)\sin(\beta) + \cos(\beta) + \cos(\alpha+\beta)] \end{aligned} \tag{15}$$

A further expression for I_{out} can be obtained by noting that the rectifier ceases conducting when $i_{Ls}(\pi-\alpha-\beta) = i_{Lp}(\pi-\alpha-\beta)$. Evaluating the preceding expression and rearrangement leads to

$$I_{\text{out}} = \frac{n\lambda}{\pi-\alpha}I_{\text{in}}\cdot[\sin(\beta)+\sin(\alpha+\beta)]. \tag{16}$$

The output voltage is subsequently found from Ohm's law: $V_{\text{out}} = I_{\text{out}}R_L$.

The fundamental component of v_{Lp} is obtained by extracting the fundamental component from a Fourier series expansion of (11),

$$\begin{aligned} v_{Lp\_1} &= \left(\frac{2nV_{\text{out}}}{\pi}[\sin(\alpha+\beta)+\sin(\beta)] + \frac{\omega L_P I_{\text{in}}}{2\pi}\right. \\ &\quad \left.\times\,[2\alpha+\sin(2\alpha+2\beta)-\sin(2\beta)]\right)\cos(\theta) \\ &\quad + \left(\frac{2nV_{\text{out}}}{\pi}[\cos(\alpha+\beta)+\cos(\beta)] + \frac{\omega_s L_P I_{\text{in}}}{2\pi}\right. \\ &\quad \left.\times\,[\cos(2(\alpha+\beta))-\cos(2\beta)]\right)\sin(\theta). \end{aligned} \tag{17}$$

As before, the equivalent impedance is found by dividing by the input current. After some manipulation, this gives

$$Z_{\text{eq}} = \frac{\omega_s L_p}{\pi}(R_{\text{eq}} + jX_{\text{eq}}) \tag{18}$$

where

$$\begin{aligned} R_{\text{eq}} &= \frac{2}{\pi-\alpha}[\sin(\alpha+\beta)+\sin(\beta)] \\ &\quad \times[\cos(\alpha+\beta)+\cos(\beta)] \\ &\quad + \frac{1}{2}[\cos(2(\alpha+\beta))-\cos(2\beta)] \\ X_{\text{eq}} &= \frac{2}{\pi-\alpha}[\sin(\alpha+\beta)+\sin(\beta)]^2 \\ &\quad + \frac{1}{2}[2\alpha+\sin(2(\alpha+\beta))-\sin(2\beta)]. \end{aligned}$$

Finally, the commutation angles α and β are found by solving two nonlinear simultaneous equations that are obtained by equating the rectifier voltage and current for specific conditions that are known to commutate the rectifier. Thus, the first equation, which accounts for the turn-off condition, is obtained by equating (15) with (16) to give

$$\begin{aligned} 0 &= \frac{2}{2\pi\lambda + (\alpha-\pi)^2}[(\pi-\alpha)\sin(\beta) \\ &\quad + \cos(\beta) + \cos(\alpha+\beta)] \\ &\quad - \frac{1}{\pi-\alpha}[\sin(\beta)+\sin(\alpha+\beta)]. \end{aligned} \tag{19}$$

$$v_{Lp}(\theta) = \begin{cases} nV_{\text{out}} & 0 < \theta \le \pi-\alpha-\beta \\ \omega_s L_p I_{\text{in}}\cos(\theta) & \pi-\alpha-\beta < \theta \le \pi-\beta \\ -nV_{\text{out}} & \pi-\beta < \theta \le 2\pi-\alpha-\beta \\ \omega_s L_p I_{\text{in}}\cos(\theta) & 2\pi-\alpha-\beta < \theta \le 2\pi-\beta \\ nV_{\text{out}} & 2\pi-\beta < \theta \le 2\pi \end{cases}. \tag{11}$$

$$i_{Lp}(\theta) = \begin{cases} i_{Lp1}(\theta) = \frac{nV_{\text{out}}}{\omega_s L_p}\theta + i_{Lp}(0) & 0 \le \theta < \pi-\alpha-\beta \\ i_{Lp2}(\theta) = I_{\text{in}}\sin(\theta) + i_{Lp}(1) & \pi-\alpha-\beta \le \theta < \pi-\beta \\ i_{Lp3}(\theta) = -\frac{nV_{\text{out}}}{\omega_s L_p}(\theta-\pi-\beta) + i_{Lp}(2) & \pi-\beta \le \theta < 2\pi-\alpha-\beta \\ i_{Lp4}(\theta) = I_{\text{in}}\sin(\theta) + i_{Lp}(3) & 2\pi-\alpha-\beta \le \theta < 2\pi-\beta \\ i_{Lp5}(\theta) = \frac{nV_{\text{out}}}{\omega_s L_p}(\theta-2\pi-\beta) + i_{Lp}(4) & 2\pi-\beta \le \theta < 2\pi \end{cases} \tag{12}$$

TABLE I
PROTOTYPE CONVERTER PARAMETERS

V_{dc}	V_{out}	L_s	L_p	C_s	n	C_f
42V	12V	7.6μH	9.7μH	138nF	1.64	100μF

The second equation is found by noting that for the rectifier to turn-on $|v_{Lp}| \geq nV_{\rm out}$. Substituting for v_{Lp} and $V_{\rm out}$, and after suitable manipulation, this leads to

$$0 = \frac{1}{\pi - \alpha}[\sin(\alpha + \beta) + \sin(\beta)] - \cos(\beta). \qquad (20)$$

C. Boundary of Continuous-Discontinuous i_R Conduction

The boundary condition for continuous rectifier current operation occurs when $|v_{Lp}|$ is just sufficient to turn-on the rectifier, immediately after a turn-off commutation. Assuming continuous current operation, one can see that the rectifier turns-off when $\theta = \pi - \alpha$. Immediately after turn-off, $|v_{Lp}(\pi - \alpha + \xi)|$ must be greater than $V_{\rm out}$ for the rectifier to turn-on again; where the angle $\xi \to 0$. Mathematically, this can be written as $-\omega_s L_p I_{\rm in} \cos(\pi - \alpha) \geq nV_{\rm out}$. Thus, the model describing continuous rectifier current operation should be employed when

$$\lambda \geq \frac{2}{\pi}. \qquad (21)$$

IV. MODEL VALIDATION

To demonstrate the prediction accuracy of the proposed models, a prototype 100 W, 42–12 V, half-bridge CLL converter, with a center-tapped transformer-rectifier, has been constructed. The converter is chosen to nominally operate at 150 kHz by selecting this as the load-independent point, and to exhibit discontinuous rectifier current for 4.5 Ω and 6 Ω loads when operated at frequencies beyond this. The converter's component parameters are listed in Table I. A series resistance of 200 m Ω is included to incorporate the effects of the transformer winding resistance and MOSFET $r_{ds(\rm on)}$.

The prediction performance of the proposed equivalent circuit models is validated against PLECS® [17] time-domain simulations, and measurements from the prototype converter, in Figs. 4 and 5, where it can be seen that models provide accurate predictions of behavior. Fig. 4 also shows the improvement in prediction accuracy over FMA techniques for lighter loads.

V. NORMALIZED ANALYSIS OF THE CLL VO CONVERTER

Here, normalized voltage and current relationships are developed from the above equivalent circuit models, which are subsequently used to determine appropriate converter parameters (Q_s, A) to meet a particular design requirement. Throughout, voltage relationships are given with respect to $V_{\rm dc}$ and are symbolized by the letter M. Current relationships are normalized with regard to $I_{\rm in}$ and are symbolized by the letter J.

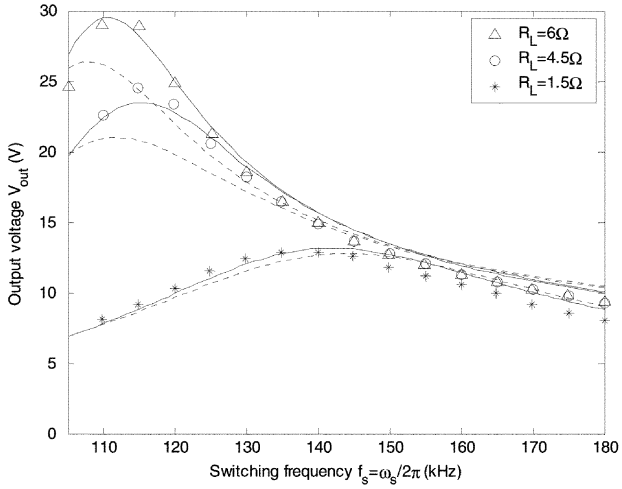

Fig. 4. Comparison between proposed model (continuous lines), FMA circuit model (broken lines), and PLECS simulation (markers).

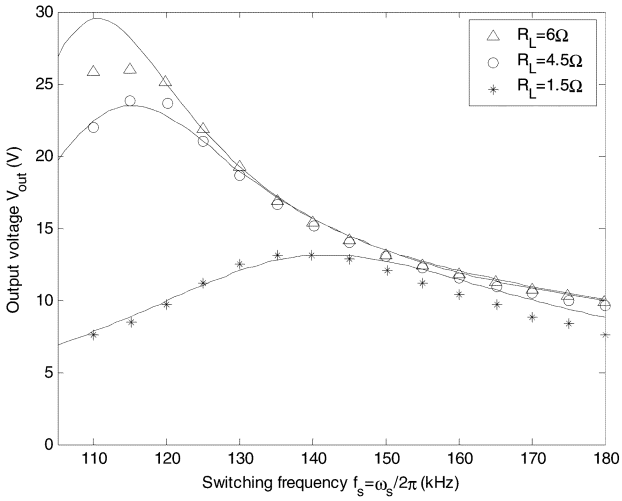

Fig. 5. Comparison between proposed model (lines) and experimental converter (markers).

A. $V_{\rm out}$ to $V_{\rm dc}$ Voltage Gain—$M_{\rm out}$

The voltage gain of the whole circuit for the standard converter parameters is obtained by substituting an expression for the input current $I_{\rm in}$ into the output voltage equation. For continuous operation, this involves (5)–(7) and (9) and additionally, for discontinuous operation (16) and (18). After appropriate manipulation, $M_{\rm out}$ can be shown to be

$$M_{\rm out} = \frac{nV_{\rm out}}{V_{\rm dc}} = \begin{cases} \frac{4\cos(\alpha)}{\pi^2} \frac{1}{\left|Z_{\rm eq1} + jQ_s\left(\omega_n - \frac{1}{\omega_n}\right)\right|}, & \lambda \geq \frac{2}{\pi} \\ \frac{2}{\pi(\pi - \alpha)} \frac{\sin(\alpha+\beta)+\sin\beta}{\left|\frac{Z_{\rm eq2}}{\pi} + j\frac{1}{A}\left(1 - \frac{1}{\omega_n^2}\right)\right|}, & \lambda < \frac{2}{\pi} \end{cases} \qquad (22)$$

where

$$Z_{\rm eq1} = \frac{8\cos(\alpha)}{\pi^2} e^{j\alpha}, Z_{\rm eq2} = R_{\rm eq} + jX_{\rm eq}, \omega_n = \frac{\omega_s}{\omega_{0s}}.$$

Fig. 6 shows example $M_{\rm out}$ as a function of ω_n for a selection of Q_s and A values. It is notable that as Q_s decreases, so does the peak gain of the converter. Secondly, the frequency at which

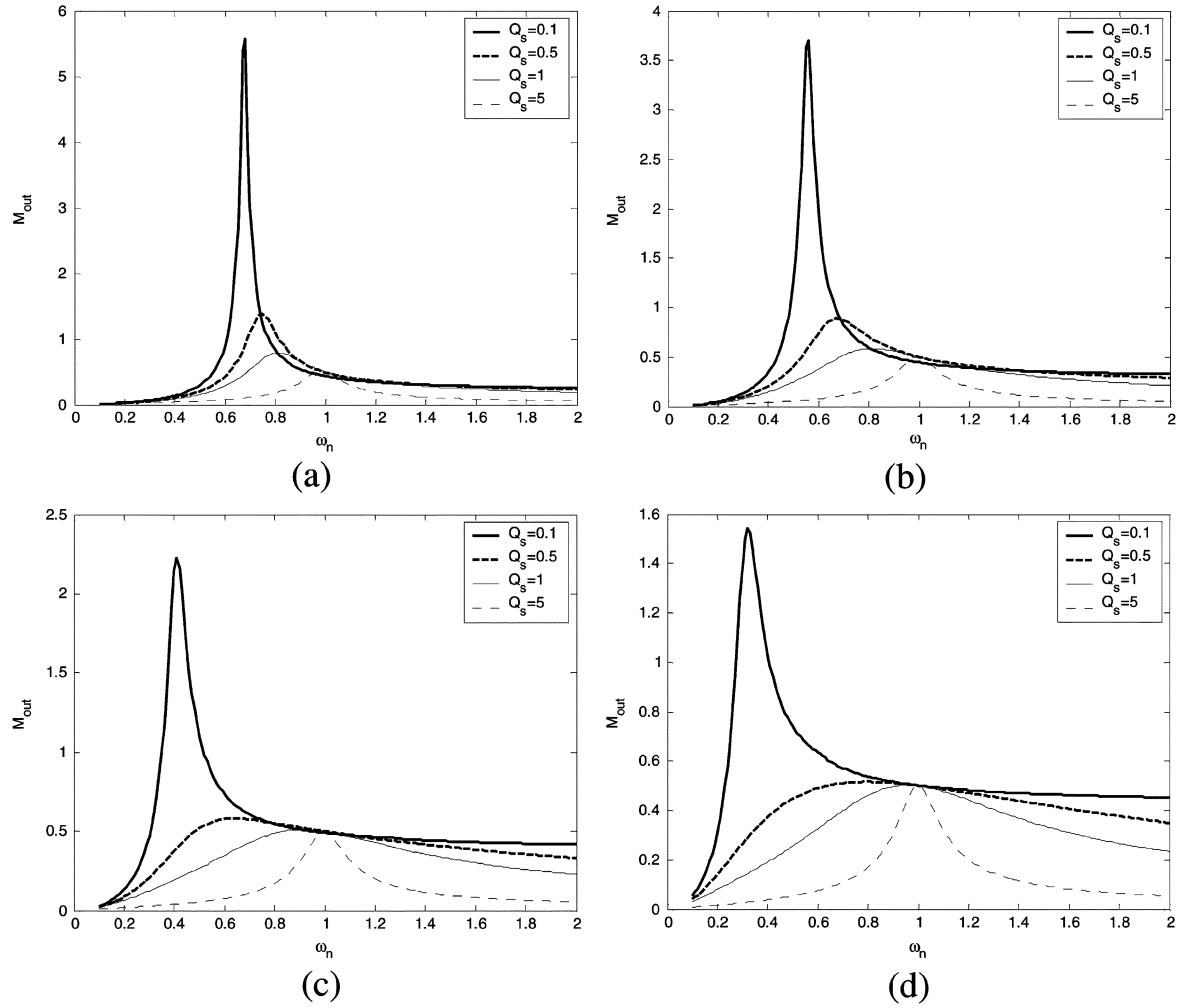

Fig. 6. $M_{\rm out}$ as a function of ω_n for various Q_s values. (a) $A = 1$, (b) $A = 2$, (c) $A = 5$, and (d) $A = 10$.

peak voltage occurs is proportional to Q_s. Also, when $\omega_n = 1$ the converter has a gain of 0.5 for all A and Q_s values—this is considered to be the load independent point. Finally, the inductor ratio A has a significant effect on the $M_{\rm out}$. Specifically, as A increases the effective voltage gain reduces. Indeed, for very large values of A and Q_s, the circuit exhibits typical series resonant converter (SRC) type behavior.

B. $I_{\rm out}$ to $I_{\rm in}$ Current Gain—$J_{\rm out}$

An expression for $J_{\rm out}$ is obtained by rearranging (5) and (14) to give

$$J_{\rm out} = \frac{I_{\rm out}}{nI_{\rm in}} = \begin{cases} \frac{2\cos(\alpha)}{\pi} & \lambda \geq \frac{2}{\pi} \\ \frac{\lambda}{(\pi-\alpha)}[\sin(\alpha+\beta)+\sin\beta] & \lambda < \frac{2}{\pi} \end{cases}. \tag{23}$$

Fig. 7 shows example $J_{\rm out}$ as a function of ω_n in a similar manner to Fig. 6. To make the comparison more tractable for "real-world" designs, $I_{\rm in}$ is converted to a rms value by dividing by $\sqrt{2}$. The series of curves clearly demonstrate that as both A and Q_s are increased there is increased coupling between the output and the input. Indeed, for large values the converter tends towards SRC type behavior once again (i.e., L_p is prohibitively large so that negligible current flows through it).

Other useful voltage and current relationships for the resonant circuit components are given in the Appendix—derived by similar procedures.

C. Practical Considerations

From the presented results, for efficient converter operation, a high $J_{\rm out}$ is sought, thereby reducing the current flowing into the resonant tank, and hence, their associated losses. This can be achieved by designing for a large A and operating about the load independent point (L.I.P.). However, in practice, this can be problematic if the converter has to operate over a large input voltage and load range. Moreover, large A ratios are often difficult to achieve when employing integrated magnetic components, and, also, the rectifier is ultimately hard switched, leading EMI concerns. A compromise is therefore often necessary—converter parameters (Q_s, A, n) are required so that the converter gain is maintained while reducing the losses. This task is not trivial given that the converter has limited voltage gain capabilities for given parameters. By way of example, Fig. 8 shows the maximum permissible voltage gain that can be obtained for several values of A, as a function of Q_s. Often,

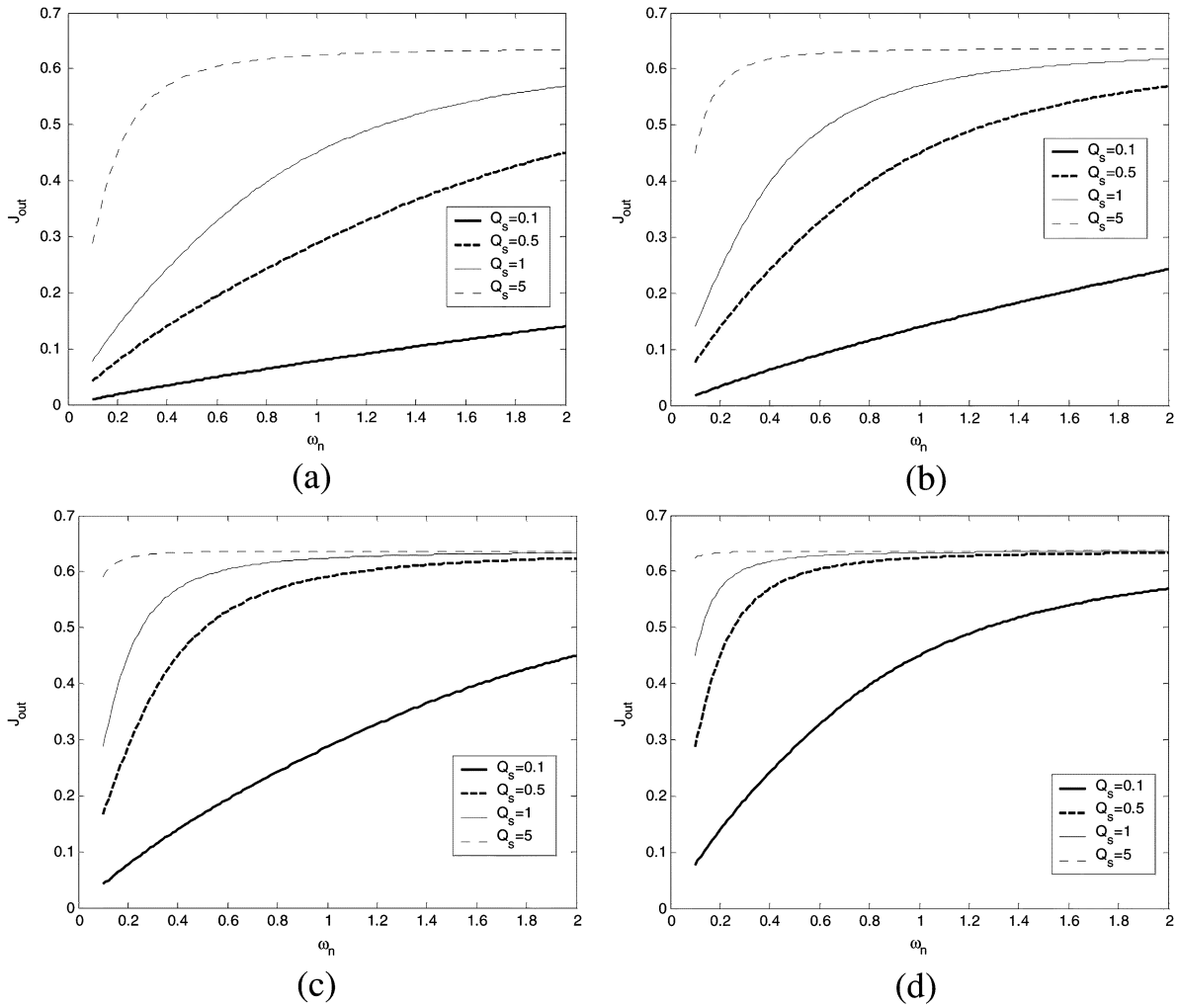

Fig. 7. $J_{\rm out}$ as a function of ω_n for various Q_s values. (a) $A = 1$, (b) $A = 2$, (c) $A = 5$, and (d) $A = 10$.

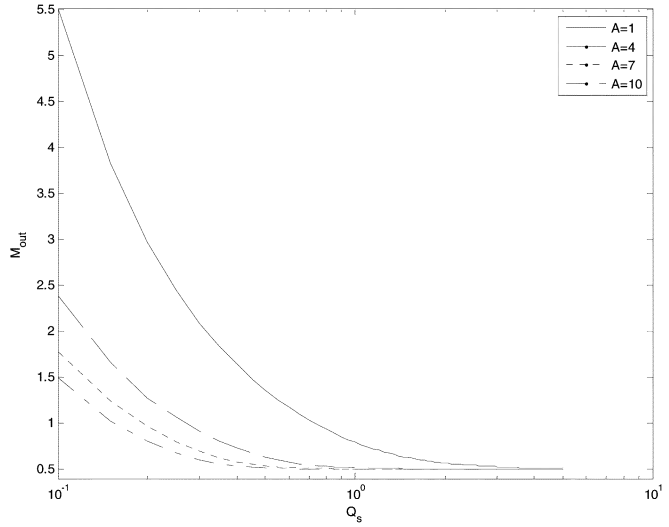

Fig. 8. Converter gain as a function of series Q-factor for numerous inductor ratios.

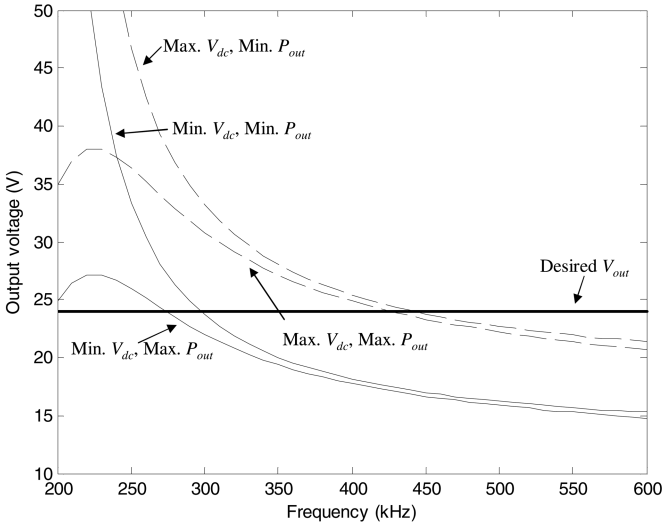

Fig. 9. Example of a typical converter frequency response used for parameter evaluation.

therefore the design procedure can require many iterations. Nevertheless, the overhead can be reduced by examining the converter's frequency response to see if the output voltage is satisfied given the extremities of output power $(P_{\rm out})$ and input voltage $(V_{\rm dc})$ ranges, see Fig. 9 for instance. One way to approach this problem could be to constrain switching frequency

TABLE II
ERROR MAP PARAMETER RANGE

Q_s	A	Z_0	f_{0s}	f_s
0.1-10	1-10	0.1-10Ω	100-500kHz	0.5-1.5×f_{0s}

under max. $V_{\rm dc}$, min. $P_{\rm out}$ operating condition to the series resonant frequency and then determine converter parameters that allow the worst case operating condition to be achieved simultaneously.

VI. MODEL BOUNDARIES

Converter models have a limited range of applicability owing to the approximations made during their derivation. This is particularly true of those derived using describing function techniques, and where it is known that the underlying system characteristics can significantly change over the operating envelope. For resonant systems in particular, as the converter is worked over its nominal operating range (and beyond) the resonant tank waveshapes can change significantly. It is therefore prudent to give boundaries of model applicability. Due to significant complexity involved in determining these boundaries, a similar technique to that reported in [14], is taken, where many randomly generated converter designs are simulated using accurate time-domain based models, the results of which are used to validate the describing function models over a wide parameter range. Notably, the normalized design parameters are used, thereby providing generically applicable results for a wide range of converter specifications.

Employing a random number generator, converter component values and an operating point is chosen from the parameter range indicated in Table II. The resulting converter design is then simulated using PLECSs®, a Matlab®/Simulink® power electronics toolbox. The filter capacitor for this model is chosen to provide a ripple voltage within 0.25% of the output voltage predicted by the proposed model. Effectively, the charge flowing into the capacitor over a given time period is equated to its voltage rise using sinusoidal approximations. The resulting PLECS model is subsequently simulated for 50× the output filter time constant. Finally, the output of the PLECS simulation is used to generate an error voltage that is plotted as a function of normalized parameters—see Fig. 10. Owing to the large number of designs considered (over 100 000) the parameter space on each error map is divided into a grid, with each pixel representing the level of prediction error (from 0% to 10%); the pixel value being determined by the average "error" within each element of the grid. The prediction error for an individual simulation is calculated from

$$V_{\rm error} = \frac{|V_{\rm out} - V_{\rm out\_Plecs}|}{V_{\rm out\_Plecs}} \times 100\%. \qquad (24)$$

Fig. 10(a) shows the variation in prediction error as a function of switching frequency and converter gain. Generally, the greatest concentration of results follow the frequency characteristics of the gain curves presented in Fig. 6. However, it can also be seen that definite boundaries exists where either the predictions are considered unreliable or where the converter parameters provide designs whose projected performance is outside the confidence tolerances. It is clear that for gains greater than 0.5, the converter must be operated below the series resonant frequency. The speckling effect seen at high conversion ratios is due to the high sensitivity of the measurements as a consequence of low Q-factors. For completeness, an error map based on predictions using a FMA equivalent circuit model is also presented [Fig. 10(b)] highlighting the improvement in prediction accuracy at light loads which is achievable using the proposed describing function model.

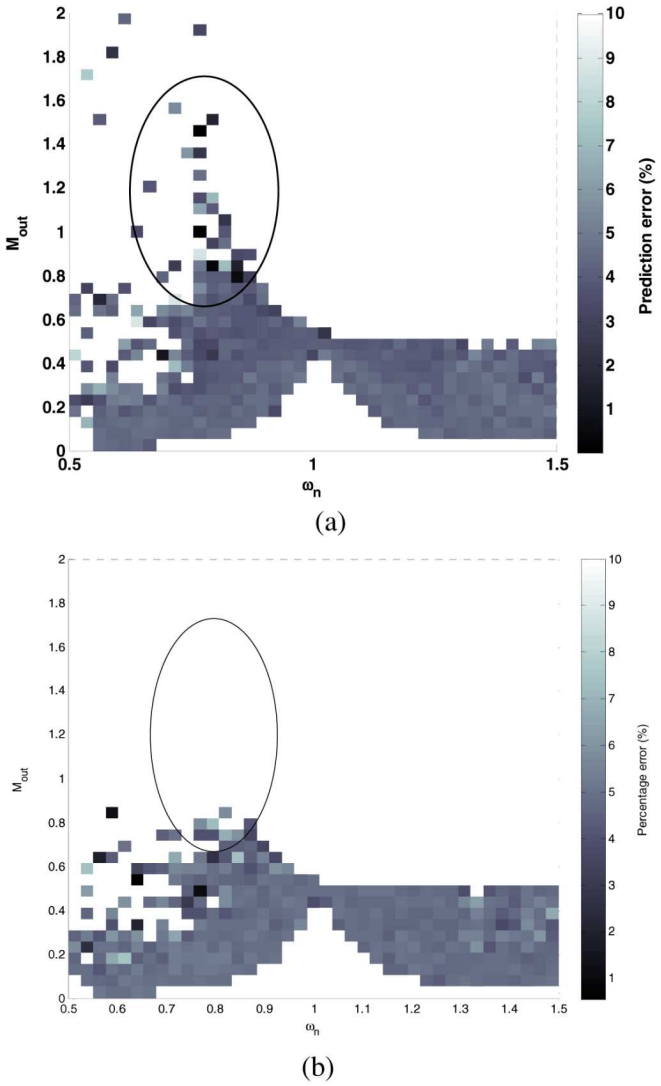

Fig. 10. Error map of converter gain against normalized switching frequency. (a) Proposed equivalent circuit model. (b) FMA equivalent circuit model.

A plot of gain versus series Q-factor is given in Fig. 11. It can be seen that for $Q_s > 2$ the maximum gain that can be achieved is 0.6 or less. Thus, somewhat counter intuitively owing to the series resonant circuit definition of Q-factor, to achieve high gains, low values of Q_s are necessary. The figure also shows that a "minimum gain boundary" exists—therefore for converter gains less than 0.4, Q_s should be restricted.

In addition to determining model applicability boundaries, the error maps are useful as an indication of design accuracy,

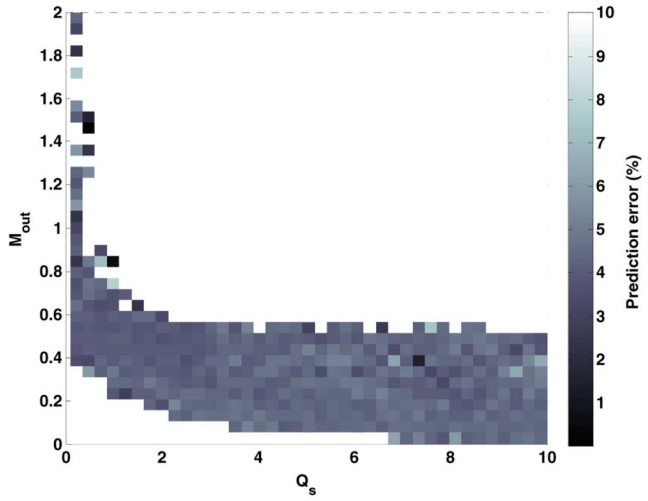

Fig. 11. Error map of converter gain against series Q-factor.

or the probable robustness of designs. For example, by placing a marker on a plot whose location corresponds to the converter's parameters, a qualitative appreciation of the projected accuracy of a converter design, i.e., a confidence measure, can be made. A more detailed treatment on the use of such error maps can be found in [10].

VII. Conclusion

Based on describing function techniques, a model for the CLL voltage-output converter operating with continuous and discontinuous rectifier currents, has been developed. By employing more precise waveshape descriptions of the rectifier current and parallel inductor voltage, the models offer improved prediction accuracy over traditional FMA based techniques, as demonstrated by a comparison of results from time-domain simulations and measurements from a prototype converter. Normalized voltage conversion ratio, and resonant circuit to output current ratios, have been developed using the derived models. These ratios provide the designer with useful information regarding permissible voltage gain and current coupling. Furthermore, design recommendations based on these ratios have also been provided. Finally, error maps that have been generated using comparisons of over 100 000 time-domain based simulations that have been employed to investigate the models' accuracy and parameter boundaries.

Appendix I

Rectifier current relationship J_R

$$J_R = \frac{i_R}{nI_{\rm in}} = \begin{cases} \left|1 - \frac{Z_{\rm eq1}}{j\lambda}\right|, & \lambda \geq \frac{2}{\pi} \\ \left|1 + j\frac{Z_{\rm eq2}}{\pi}\right|, & \lambda < \frac{2}{\pi} \end{cases}.$$

Series capacitor voltage relationship $M_{\rm Cs}$

$$M_{\rm Cs} = \frac{v_{\rm Cs}}{V_{\rm dc}} = \begin{cases} \frac{2Q_s}{\pi\omega_n}\frac{1}{Q_s\left(\frac{1}{\omega_n}-\omega_n\right)+jZ_{\rm eq1}}, & \lambda \geq \frac{2}{\pi} \\ \frac{2}{\pi A\omega_n^2}\frac{1}{\frac{1}{A}\left(\frac{1}{\omega_n^2}-1\right)+j\frac{Z_{\rm eq2}}{\pi}}, & \lambda < \frac{2}{\pi} \end{cases}.$$

Series inductor voltage relationship M_{Ls}

$$M_{Ls} = \frac{v_{Ls}}{V_{\rm dc}} = \begin{cases} \frac{2Q_s}{\pi}\omega_n\frac{j}{Z_{\rm eq1}+jQ_s\left(\omega_n-\frac{1}{\omega_n}\right)}, & \lambda \geq \frac{2}{\pi} \\ \frac{2}{\pi A}\frac{j}{\frac{Z_{\rm eq2}}{\pi}+j\frac{1}{A}\left(1-\frac{1}{\omega_n^2}\right)}, & \lambda < \frac{2}{\pi} \end{cases}$$

Parallel inductor current ratio J_{Lp}

$$J_{Lp} = \frac{i_{Lp}}{I_{\rm in}} = \begin{cases} \frac{Z_{\rm eq1}}{j\lambda}, & \lambda \geq \frac{2}{\pi} \\ \frac{Z_{\rm eq2}}{j\pi}, & \lambda < \frac{2}{\pi} \end{cases}.$$

Parallel inductor voltage ratio M_{Lp}

$$M_{Lp} = \frac{v_{Lp}}{V_{\rm dc}} = \begin{cases} \frac{2}{\pi}\frac{Z_{\rm eq1}}{Z_{\rm eq1}+jQ_s\left(\omega_n-\frac{1}{\omega_n}\right)}, & \lambda \geq \frac{2}{\pi} \\ \frac{2}{\pi^2}\frac{Z_{\rm eq2}}{\frac{Z_{\rm eq2}}{\pi}+j\frac{1}{A}\left(1-\frac{1}{\omega_n^2}\right)}, & \lambda < \frac{2}{\pi} \end{cases}.$$

References

[1] W.-Y. Choi, J.-M. Kwon, and B.-H. Kwon, "High-performance front-end rectifier system for telecommunication power supplies," *Proc. Inst. Elect. Eng.*, vol. 153, no. 4, pp. 473–482, Jul. 2006.

[2] M. G. Egan, D. L. O'Sullivan, J. G. Hayes, M. J. Willers, and C. P. Henze, "Power-factor-corrected single-stage inductive charger for electric vehicle batteries," *IEEE Trans. Ind. Electron.*, vol. 54, no. 2, pp. 1217–1226, Apr. 2007.

[3] K. Jin and X. Ruan, "Hybrid full-bridge three-level LLC resonant converter-a novel DC-DC converter suitable for fuel-cell power system," *IEEE Trans. Ind. Electron.*, vol. 53, no. 5, pp. 1492–1503, Oct. 2006.

[4] M. Borage, S. Tiwari, and S. Kotaiah, "Constant-current, constant-voltage half-bridge resonant power supply for capacitor charging," *IET Elect. Power Applic.*, vol. 153, no. 3, pp. 343–347, May 2006.

[5] A. K. S. Bhat, "Analysis and design of LCL-type series resonant converter," *IEEE Trans. Ind. Electro.*, vol. 41, no. 1, pp. 118–124, Feb. 1994.

[6] R. L. Steigerwald, "A comparison of half-bridge resonant converter topologies," *IEEE Trans. Power Electron.*, vol. 3, no. 2, pp. 174–182, Apr. 1988.

[7] M. K. Kazimierczuk and D. Czarkowski, *Resonant Power Converters*. New York: Wiley, Apr. 1995.

[8] I. Batarseh, "State-plane approach for the analysis of half-bridge parallel resonant converters," *Proc. Inst. Elect. Eng.*, vol. 142, no. 3, pp. 200–204, Jun. 1995.

[9] A. K. S. Bhat, "Analysis and design of a series-parallel resonant converter with capacitive output filter," *IEEE Trans. Ind. Appl.*, vol. 27, no. 3, pp. 523–530, May/Jun. 1991.

[10] J. F. Lazar and R. Martinelli, "Steady-state analysis of the LLC series resonant converter," in *Proc. IEEE Appl. Power Electron. Conf. Expo.*, 2001, vol. 2, pp. 728–735.

[11] A. J. Forsyth and S. V. Mollov, "Simple equivalent circuit for the series-loaded resonant converter with voltage boosting capacitor," *Proc. Inst. Elect. Eng.*, vol. 145, no. 4, pp. 301–306, Jul. 1998.

[12] J. G. Hayes and M. G. Egan, "Rectifier-compensated fundamental mode approximation analysis of the series-parallel LCLC family of resonant converters with capacitive output filter and voltage-source load," in *Proc. IEEE Power Electron. Spec. Conf.*, 1999, vol. 2, pp. 1030–1036.

[13] H. I. Sewell, M. P. Foster, C. M. Bingham, D. A. Stone, D. Hente, and D. Howe, "Analysis of voltage output LCC resonant converters, including boost mode operation," *Proc. Inst. Elect. Eng.*, vol. 150, no. 6, pp. 673–679, Nov. 2003.

[14] M. P. Foster, H. I. Sewell, C. M. Bingham, D. A. Stone, and D. Howe, "Methodologies for the design of LCC voltage-output resonant converters," *Proc. Inst. Elect. Eng.*, vol. 153, no. 4, pp. 559–567, Jul. 2006.

[15] A. J. Forsyth, G. A. Ward, and S. V. Mollov, "Extended fundamental frequency analysis of the LCC resonant converter," *IEEE Trans. Power Electron.*, vol. 18, no. 6, pp. 1286–1292, Nov. 2003.

[16] G. Ivensky, S. Bronstein, and S. Ben-Yaakov, "Approximate analysis of the resonant LCL DC-DC converter," in *Proc. IEEE Israel Convention*, 2004, pp. 44–48.

[17] [Online]. Available: http://www.plexim.com/PLECS toolbox, Plexim

Martin P. Foster received the B.Eng. degree in electronic and electrical engineering, the M.Sc. (Eng.) degree in control systems, and the Ph.D. degree in 1998, 2000, and 2003, respectively, all from the University of Sheffield, Sheffield, U.K.

In 2003, he became a Member of Academic Staff at the University of Sheffield, specializing in power electronic systems. His current research interests include the modelling and control of switching power converters, resonant power supplies, lightweight energy transformation components, power electronic packaging, and autonomous aerospace vehicles.

Dr. Foster received an award for his Ph.D. dissertation "Analysis and design of high-order resonant power converters" from the University of Sheffield.

Christopher R. Gould received the M.Eng. degree in electronic and electrical engineering with communications in 2002 and the Ph.D. degree in 2006, both from the University of Sheffield, Sheffield, U.K.

Since 2005, he has been a Research Associate in the Electrical Machines and Drives Group, Department of Electronic and Electrical Engineering, University of Sheffield. His current research interests include the modeling and control of resonant power supplies, battery management systems and battery state-of-charge/health modelling for all-electric steer-by wire vehicles, and the design of efficient brushless ac motor for sensorless control of electric mobility vehicles.

Dr. Gould received an Award for his Ph.D. dissertation "Rapid analysis and design of CLL resonant power converters" from the University of Sheffield.

Adam J. Gilbert received the M.Eng. and Ph.D. degrees in electronic and electrical engineering from the University of Sheffield, Sheffield, U.K., in 2002 and 2008, respectively.

His research interests include the modeling and control of switching power converters with particular emphasis on high-efficiency resonant supplies.

David A. Stone received the B.Eng. degree in electronic engineering from the University of Sheffield, Sheffield, U.K., in 1985 and the Ph.D. degree from Liverpool University, Liverpool, U.K., in 1989.

He then returned to the University of Sheffield as a Member of Academic Staff specializing in power electronics and machine drive systems. His current research interests are in hybrid-electric vehicles, battery charging, EMC, and novel lamp ballasts for low-pressure fluorescent lamps.

Christopher M. Bingham received the B.Eng. degree in electronic systems and control engineering from Sheffield City Polytechnic, Sheffield, U.K., in 1989, the M.Sc. (Eng.) degree in control systems engineering from the University of Sheffield, Sheffield, U.K., in 1990, and the Ph.D. degree in control systems to accommodate nonlinear dynamic effects in aerospace flight-surface actuators from Cranfield University, Shrivenham, U.K., in 1994.

He remained at Cranfield University as a Post-Doctoral Researcher until subsequently taking up a research position at the University of Sheffield. Since 1998, he has been a Lecturer in the Department of Electronic and Electrical Engineering, University of Sheffield. His current research interests include traction control/anti-lock braking systems for electric vehicles, electro-mechanical actuation of flight control surfaces, control of active magnetic bearings for high-speed machines, sensorless control of brushless machines, analysis and design of resonant converter systems, and the control of high-performance UAVs.